An Adjoint Sensitivity Study of Buoyancy- and Wind-Driven Circulation on the New Jersey Inner Shelf

WEIFENG G. ZHANG, JOHN L. WILKIN, JULIA C. LEVIN, AND HERNAN G. ARANGO

Institute of Marine and Coastal Sciences, Rutgers, The State University of New Jersey, New Brunswick, New Jersey

ABSTRACT

Adjoint sensitivity analysis is used to study the New York Bight circulation for three idealized situations: an unforced buoyant river plume, and upwelling and downwelling wind forcing. A derivation of adjoint sensitivity is presented that clarifies how the method simultaneously addresses initial, boundary, and forcing sensitivities. Considerations of interpretation and appropriate definitions of sensitivity scalar indices are discussed. The adjoint method identifies the oceanic conditions and forcing that are "dynamically upstream" to a region or feature of interest, as well as the relative roles of the prior ocean state, forcing, and dynamical influences. To illustrate the method, which is quite general, the authors consider coastal sea surface temperature (SST) variability and define the adjoint scalar index as the temporal–spatial mean squared SST anomaly on a segment of the New Jersey coast at the conclusion of a 3-day period. In the absence of wind, surface temperature advection dominates the SST anomaly with two sources of surface water identified. Downwelling winds amplify upstream advective influence. Sensitivity to temperature is separated into direct advection and the dynamic effect on density stratification and mixing. For upwelling conditions, this decomposition shows that coastal SST is controlled by both advection from the south and subsurface, but above the 5-m depth, and temperature-related density stratification between 5 and 15 m to 10 km offshore. By identifying the timing and location of ocean conditions crucial to subsequent prediction of specific circulation features, the adjoint sensitivity method has application to quantitative evaluation of observational sampling strategies.

1. Introduction

The sector of the Mid-Atlantic Bight adjacent to the coast of New Jersey is separated from the slope sea by a wide, shallow shelf, largely insulating the circulation of the New Jersey inner shelf from remotely generated deep ocean forcing. Historical observations show that ocean variability in the area is most energetic at relatively short time and space scales, further suggesting likely dominance by local forcing. In recent years, the region has been the focus of studies designed to examine the dynamics of wind-driven coastal upwelling and buoyancy-driven coastal currents (Choi and Wilkin 2007; Johnson et al. 2003; Münchow and Chant 2000; Tilburg and Garvine 2003; Wong 1999; Yankovsky and Garvine 1998; Yankovsky et al. 2000). These studies indicate that tides, river runoff, and air–sea exchanges all exert influence with no single forcing mechanism

controlling the regional dynamics. Details of the coastline (Yankovsky 2003; Yankovsky and Garvine 1998) and bathymetry variations (Chant et al. 2004; Garvine 2004; Kohut et al. 2004) also affect the local ocean response.

Using in situ observations on the New Jersey inner shelf, Yankovsky and Garvine (1998) first found the interaction between wind-driven coastal upwelling and buoyancy intrusions; Wong (1999) discovered cross-shelf inhomogeneity in the ocean's reaction to wind and attributed it to the buoyancy-driven coastal current on the inner shelf; Yankovsky et al. (2000) showed the spatial variability of mesoscale currents driven by the interaction of buoyancy and wind; Chant (2001) concluded that near-inertial motions are mainly driven by local wind and subsequently propagate gradually into the thermocline; Tilburg and Garvine (2003) and Yankovsky (2003) both investigated the three-dimensionality of the flow generated by the combination of wind and buoyancy intrusions; Chant et al. (2004) further proved the three-dimensionality of the wind-driven flow by studying coastal flow reversals during upwelling conditions;

Corresponding author address: Weifeng G. Zhang, 71 Dudley Road, New Brunswick, NJ 08901.
E-mail: zhang@marine.rutgers.edu

Johnson et al. (2003) described two dynamic states of the coastal ocean—a river plume state and an upwelling state; Garvine (2004) investigated the influence of buoyancy intrusion and wind forcing on the vertical structure of the flow, especially the thickness of surface mixed layer and bottom mixed layer; Kohut et al. (2004) demonstrated strong correlation between wind and surface current on seasonal scales; and Castelao et al. (2008) identified the local wind as a significant role player in driving coastal dynamics and spreading the plume. In numerical model studies, Choi and Wilkin (2007) concluded that wind and, to a lesser extent, buoyancy forces together determine the pattern of horizontal freshwater dispersal; and Zhang et al. (2009) identified wind as the primary force to spread river-injected freshwater onto the mid and outer shelf. All of these studies proved wind and buoyancy are two significant competing forces on the New Jersey inner shelf. Their influences on SST on the coast are exactly what we want to quantify in this study.

In several instances the interdisciplinary studies noted above pioneered deployments of new observing instruments, including autonomous gliders, surface current measuring high-frequency radar (CODAR), and a cabled observatory, with further data acquired from multiple satellites, Lagrangian dye tracking, surface drifters, moorings, and shipborne instruments. In the New York Bight the operation of many of these sensors continues on a quasi-continuous basis, and the area is presently the nation's most densely routinely observed coastal region. Consequently, this is an attractive location in which to explore the integration of advanced observation, modeling, and data assimilation capabilities for the purposes of implementing coastal ocean forecast systems.

The work presented here uses one of the variational calculus-based methods—specifically, the adjoint sensitivity technique—to identify conditions and forcing that are dynamically upstream, to quantify the relative significance of buoyancy and wind forcing to coastal dynamics in the New York Bight, and to characterize coherent patterns of circulation variability that deserve consideration in the deployment of regional coastal observing systems. Adjoint model sensitivity analysis is a step toward developing a comprehensive four-dimensional variational (4DVAR) data assimilation system that will exploit the diversity of coastal ocean observation technologies available and direct their deployment.

Over the last 5 to 10 years there has been a significant expansion in the application of variational methods in oceanography for data assimilation. One crucial component that underlies the variational assimilation approach is the adjoint model or, more precisely, the adjoint of a tangent linear approximation to a conventional forward ocean simulation model. In addition to data assimilation, other applications of the adjoint model include parameter estimation, stability analysis, sensitivity analysis, and optimal observation network design (Moore et al. 2004). Beginning in the 1980s, meteorologists established the theory of adjoint sensitivity and used it to study how selected features of a model forecast vary with respect to prior model states (Errico and Vukicevic 1992). More recently, adjoint sensitivity studies have been applied in oceanography (Dutkiewicz et al. 2006; Galanti and Tziperman 2003; Hill et al. 2004; Junge and Haine 2001; Li and Wunsch 2004; Losch and Heimbach 2007; Marotzke et al. 1999; van Oldenborgh et al. 1999) but with a focus on mesoscale to gyre-scale physics in ocean general circulation models. In one of the first coastal ocean applications, albeit still in the predominantly deep waters of the California Current System, Moore et al. (2009) examined how coastal upwelling, eddy kinetic energy variability, and baroclinic instability are affected by surface forcing. In this paper, a related adjoint sensitivity approach is applied, but to a different class of analyses.

On the New Jersey inner shelf the prior ocean state influences how the ocean responds to direct forcing: quite different ocean responses can occur under similar forcing conditions if the oceanic preconditioning differs. In adjoint sensitivity analysis, oceanic response is characterized by some particular aspect of the model variation expressed in terms of a user-defined scalar functional. The analysis quantifies how this aspect of the model varies with respect to initial conditions and forcing over some finite time interval. The methodology is effective at revealing the spatial and temporal extent of the oceanic conditions and forcing that are "dynamically upstream" to a region or feature of interest. In this paper, we emphasize how this analysis approach is a tool for addressing two questions that frequently drive observing system design: (i) Can we quantify the aspects of the ocean state that dominate the dynamics under differing circulation conditions and (ii) can we identify the most useful places and times at which to make observations so as to better estimate the true ocean state?

There are a number of challenges to adjoint modeling in limited-area coastal domains. The first is open boundary conditions, which are formally ill posed in any nonlinear forward model and can become worse in an adjoint model. This is because any information that propagates out of the open boundaries in the forward tangent linear model is simply lost to the backward mode of the adjoint, unless tangent linear model states on the

open boundaries are stored completely. Nonlinearity of coastal currents and abrupt gradients induced by local vertical mixing can pose further difficulties. The issue here is that the adjoint model is formulated for perturbations (the tangent linear approximation) along a trajectory of the nonlinear model, and validity of the linear perturbation assumption needs to be ascertained. This study is also a demonstration of how to deal with these difficulties in practice. The technique exhibited here can also be applied to determining which features of the regional oceanography dominate other local phenomena of interest such as freshwater anomaly transport, the trajectory of a phytoplankton bloom or reactive biogeochemical component, and so on.

The outline of this paper is as follows: An alternative mathematical derivation of adjoint sensitivity is given in section 2a to better illustrate the interpretation of the adjoint variables. This is followed by an explanation of adjoint sensitivity in section 2b. Section 2c gives the definition of scalar sensitivity index J and guidelines on its formulation. The model configuration and proof of the linearization are given in section 3. Model output is presented in section 4 and summarized in section 5.

2. Adjoint sensitivity

a. An alternative derivation of adjoint sensitivity

Different approaches have been used to describe the mathematical and conceptual formalism of adjoint sensitivity. Errico (1997) combined a Taylor series expansion with a temporal discrete consideration of the model. Marotzke et al. (1999) extended this method by applying an automatic differentiation to derive an adjoint code. However, these time-step-by-time-step derivations do not give a mathematically concise form of adjoint sensitivity. The propagator-based approach, adopted by Moore et al. (2009), showed that backward in time integration of the adjoint model gives the sensitivity to initial conditions, forcing, and boundary conditions. Here, an alternative explanation also using the propagator algorithm and variational data assimilation theory is presented to show the sensitivities from a different angle.

Following Moore et al. (2004), we represent the forward ocean model as

$$
\begin{cases}
\dfrac{\partial \mathbf{\Phi}(t)}{\partial t} = M(\mathbf{\Phi}(t)) + \mathbf{F}(t) \\
\mathbf{\Phi}(0) = \mathbf{\Phi}_i \\
\mathbf{\Phi}(t)|_\Omega = \mathbf{\Phi}_\Omega(t)
\end{cases}, \qquad (1)
$$

where M is the model nonlinear operator; $\mathbf{\Phi}(t)$ is a state vector $[u \, v \, T \, S \, \zeta]^{\mathrm{T}}$ comprised of the velocity, tempera-

ture, salinity, and sea surface height at all model grid points at time t; $\mathbf{F}(t)$ is the external forcing; $\mathbf{\Phi}_i$ are the initial conditions; and $\mathbf{\Phi}_\Omega(t)$ are boundary conditions along boundary Ω. We let $\mathbf{\Phi}_0$ denote a solution to the nonlinear problem (1) and introduce perturbations $\boldsymbol{\phi}_i = \delta\mathbf{\Phi}_i$, $\boldsymbol{\phi}_\Omega(t) = \delta\mathbf{\Phi}_\Omega(t)$, and $\mathbf{f}(t) = \delta\mathbf{F}(t)$ to the initial conditions, boundary conditions, and forcing, respectively. Then, using a Taylor expansion around the base state $\mathbf{\Phi}_0$, we obtain the so-called tangent-linear model:

$$
\frac{\partial \boldsymbol{\phi}}{\partial t} = \left(\frac{\partial M}{\partial \mathbf{\Phi}}\right)\bigg|_{\mathbf{\Phi}_0} \delta\mathbf{\Phi} + \delta\mathbf{F}(t) = \mathbf{C}\boldsymbol{\phi} + \mathbf{f}(t),
$$
$$
\boldsymbol{\phi}(0) = \boldsymbol{\phi}_i, \qquad\qquad\qquad\qquad\qquad (2)
$$
$$
\boldsymbol{\phi}(t)|_\Omega = \boldsymbol{\phi}_\Omega(t),
$$

where $\boldsymbol{\phi} = \delta\mathbf{\Phi} = \mathbf{\Phi} - \mathbf{\Phi}_0$ is the departure from the base state $\mathbf{\Phi}_0$ and $\mathbf{C}$ is a linear matrix operator. When discretized in space and time, the tangent linear model yields a system of linear equations:

$$
\mathbf{A}\boldsymbol{\phi} = \mathbf{b}. \qquad (3)
$$

Here, $\mathbf{A}$ is a coefficient matrix and $\mathbf{b}$ is a rhs vector that consists of boundary conditions, initial conditions, and external forcings as

$$
\begin{bmatrix}
\cdots & \cdots & \cdots & \cdots \\
\cdots & \cdots & \cdots & \cdots \\
\cdots & c_{ij}^k & c_{ij}^{k+1} & \cdots \\
\cdots & \cdots & \cdots & \cdots
\end{bmatrix}
\begin{bmatrix}
\vdots \\
\varphi_{ij}^k \\
\varphi_{ij}^{k+1} \\
\vdots
\end{bmatrix}
=
\begin{bmatrix}
\vdots \\
\vdots \\
\hat{b}_{ij}^k + f_{ij}^k \Delta t \\
\vdots
\end{bmatrix},
$$

where φ_{ij}^k is the tangent linear state variable at the kth time step at location (i, j), c_{ij}^k is the corresponding coefficient coming from discretization and model physics, Δt is the time step, $\hat{b}_{ij}^k$ is discretized initial condition or boundary condition, and f_{ij}^k is discretized forcing. If the trivial equations $f_{ij}^k \Delta t = f_{ij}^k \Delta t$ are added to the system, matrix $\mathbf{A}$ and vector $\mathbf{b}$ can be modified to incorporate the forcing terms into the state vector; thus,

$$
\begin{bmatrix}
\cdots & \cdots & \cdots & \cdots & \cdots \\
\cdots & \cdots & \cdots & \cdots & \cdots \\
\cdots & c_{ij}^k & c_{ij}^{k+1} & \cdots & -1 \\
\cdots & \cdots & \cdots & \cdots & \cdots \\
0 & 0 & 0 & 0 & 1
\end{bmatrix}
\begin{bmatrix}
\cdots \\
\varphi_{ij}^k \\
\varphi_{ij}^{k+1} \\
\cdots \\
f_{ij}^k \Delta t
\end{bmatrix}
=
\begin{bmatrix}
\cdots \\
\hat{b}_{ij}^k \\
\cdots \\
f_{ij}^k \Delta t
\end{bmatrix}.
$$

Now, each element in the rhs vector $\mathbf{b}$ is a discretized element of initial conditions, boundary conditions, or forcing. Following Errico (1997), we define a scalar

functional J that describes a chosen aspect of the model state for which we wish to explore the sensitivity:

$$J = G(\mathbf{\Phi}(t)). \tag{4}$$

Applying the method of Lagrangian multipliers (Bertsekas 1982), we define a corresponding scalar index (or cost function for data assimilation),

$$J = G(\mathbf{\Phi}) = G(\mathbf{\Phi}) + \boldsymbol{\mu}^{\mathrm{T}}(\mathbf{A}\boldsymbol{\phi} - \mathbf{b}), \tag{5}$$

which has the same minimum as (4) for all φ that satisfy (3). Here $\boldsymbol{\phi}$ is the tangent linear state vector that incorporates $f\Delta t$, as discussed before; $\boldsymbol{\mu}$ is a vector of Lagrange multipliers; and $\mathbf{b}$ is the right-hand side of the tangent linear model including initial conditions, boundary conditions, and forcing.

Setting $\delta J/\delta \boldsymbol{\mu}$ to zero (Bennett 2002), we recover the tangent linear model (3); setting $\delta J/\delta \boldsymbol{\phi}$ to zero results in the adjoint system:

$$-\mathbf{A}^{\mathrm{T}}\boldsymbol{\mu} = \frac{\partial G}{\partial \boldsymbol{\phi}} = \frac{\partial G}{\partial (\boldsymbol{\phi} + \mathbf{\Phi}_0)} = \frac{\partial G}{\partial \mathbf{\Phi}}, \tag{6}$$

This shows that $\partial G/\partial \mathbf{\Phi}$ is the adjoint forcing, $\mathbf{A}^{\mathrm{T}}$ the adjoint operator, and the Lagrange multipliers μ are the adjoint variables. Additionally,

$$\frac{\delta J}{\delta \mathbf{b}} = \frac{\delta G}{\delta \mathbf{b}} = \boldsymbol{\mu}, \tag{7}$$

indicating that $\boldsymbol{\mu}$ are the sensitivities of J with respect to all the components of $\mathbf{b}$. In other words, the adjoint variables μ reveal how J depends on perturbations to all of the initial conditions, boundary conditions, and forward model forcing. For J defined as the mismatch between the model state and observations, the sensitivity information can be used to adjust initial conditions to obtain a better model–observation match (Courtier et al. 1994); this is the underlying principle of variational data assimilation. If J is a scalar measure of some aspect simulated in the nonlinear model, the adjoint sensitivity identifies locations and variables that are important to this feature.

b. Dimensional considerations in the physical interpretation of adjoint sensitivity

In the discrete model, a perturbation is distributed over the small yet finite-sized grid cell that contains the perturbation point. The Regional Ocean Modeling System (ROMS) (http://www.myroms.org) utilizes orthogonal curvilinear coordinates that allow for variable grid sizes that must be accounted for in the formulation in order to make the correct physical interpretation

of adjoint sensitivity. In practice, sensitivity is most readily interpreted as the gradient of J with respect to equivalent masses or volumes of water (Lewis et al. 2001). In ocean applications, mass-weighted and volume-weighted sensitivity differ little, and the latter is used in this study. The horizontal grid here is almost uniform, so we show horizontal fields of adjoint sensitivity without any scaling. However, the ROMS terrain-following vertical coordinate is stretched significantly where bathymetry varies and the consequent changes in grid cell thickness change the cell volume. Accordingly, the vertical grid cell thickness is used to scale the vertical fields of adjoint sensitivity presented in section 4.

Adjoint sensitivity allows comparison of the relative contributions of different variables to the variation of the model aspect of interest. Consider the total variation of J,

$$\delta J = \frac{\partial J}{\partial u_0}\delta u_0 + \frac{\partial J}{\partial T_0}\delta T_0 + \frac{\partial J}{\partial \tau_{x0}}\delta \tau_{x0} + \frac{\partial J}{\partial \nu_{h0}}\delta \nu_{h0} + \cdots, \tag{8}$$

where

$$\frac{\partial J}{\partial u_0}, \frac{\partial J}{\partial T_0}, \frac{\partial J}{\partial \tau_{x0}}, \frac{\partial J}{\partial \nu_{h0}} \cdots$$

are the adjoint variables (sensitivities), and δu_0, δT_0, $\delta \tau_{x0}$, $\delta \nu_{h0}$ ... are variations of forward model variables (i.e., the state variables, but also forcing) at time zero. The relative contributions of different variables to the variation of J [i.e., the respective terms in Eq. (8)] can be expressed in appropriate dimensional units by multiplying the adjoint variables by estimates of the magnitude of uncertainty in the corresponding nonlinear model variables. This procedure identifies those state variables or parameters that contribute most to the variation of J. This knowledge is readily applied to the question of determining which variables, where, and when, are crucial to obtaining a good estimate of J and therefore pertinent to directing observing system design and deployments targeted at capturing a particular event or phenomenon characterized by the appropriate J (Köhl and Stammer 2004). It should be noted that adjoint sensitivity does not immediately reveal the underlying dynamics of the event, although it might point to, or eliminate, certain event triggers at particular places or times. The real triggers will need to be identified through further model analysis.

c. Definition of the scalar index J

The scalar functional $J = G(\mathbf{\Phi}(t))$ [Eq. (4)] is defined according to the question of interest. Moore et al. (2009)

give several definitions for different applications. We would like to add two comments on defining J. First, caution should be exercised in defining J precisely targeting the aspect of interest, especially when the aspect of interest is too vague to define a J specifically. Once a particular J is chosen, the sensitivity of J with respect to initial conditions or boundary conditions ought to be interpreted precisely according to the definition. Second, the cost function in variational data assimilation is nondimensionalized by model and observation error covariance, which gives the tangent linear model variables the same units as the forward model variables. However, for adjoint sensitivity analysis, there is no necessity to nondimensionalize J because the factor would be a single constant and would make no difference to the interpretation of sensitivity patterns. In this work, J is *dimensional*.

A characteristic feature of New Jersey coastal ocean dynamics is the occurrence of wind-induced upwelling and downwelling that leads to low and high SST, respectively, along the coast (Chant 2001; Münchow and Chant 2000). We study these events here by defining a J that is the SST anomaly variance within a localized area adjacent to the New Jersey coast:

$$J = \frac{1}{2(t_2 - t_1)A} \int_{t_1}^{t_2} \int_A (T_S - \overline{T_S})^2 dA \, dt, \quad (9)$$

where T_S is SST and $\overline{T}_S$ is its temporal mean, and the definition considers the temperature anomaly within an area A during a time interval t_1 to t_2. Here, the time period is chosen to be the last three hours of the simulation time window. Note that J is defined as a quadratic form to prevent the cancellation of positive and negative anomaly inside area A.

Being a scalar that characterizes local temperature variability, J could be affected by temperature through two different mechanisms: (i) transport, that is, advection or diffusion of temperature as a tracer, and (ii) dynamics, that is, the contribution of temperature to density and thereby to baroclinic pressure gradients and stratification that impacts vertical turbulent mixing. To separate the sensitivity of J due to advection/diffusion from that due to the density effects, Marotzke et al. (1999) introduced a decomposition in which J is rewritten as a function of temperature and salinity with density and temperature as intermediates:

$$J = J(T, S) = J(q(T), \rho(T, S)). \quad (10)$$

Here $q = T$ denotes the contribution of temperature in J only when it is being advected or diffused and has no relation with salinity, which implies $\partial q/\partial T|_S = 1$ and $\partial q/\partial S|_T = 0$.

Applying the chain rule, the sensitivity of J to temperature can be expressed as

$$\begin{aligned} \left.\frac{\partial J}{\partial T}\right|_S &= \left.\frac{\partial J}{\partial q}\right|_\rho \left.\frac{\partial q}{\partial T}\right|_S + \left.\frac{\partial J}{\partial \rho}\right|_q \left.\frac{\partial \rho}{\partial T}\right|_S \\ &= \left.\frac{\partial J}{\partial q}\right|_\rho + \left.\frac{\partial J}{\partial \rho}\right|_q \left.\frac{\partial \rho}{\partial T}\right|_S \\ &= \left.\frac{\partial J}{\partial T}\right|_\rho - \alpha\rho\left.\frac{\partial J}{\partial \rho}\right|_q, \end{aligned} \quad (11)$$

where α is the thermal expansion coefficient. The first term on the rhs of (11) is the sensitivity to temperature due to the processes of advection or diffusion, whiles the second term describes the density effect. These can be separated by considering the sensitivity to salinity:

$$\left.\frac{\partial J}{\partial S}\right|_T = \left.\frac{\partial J}{\partial q}\right|_\rho \left.\frac{\partial q}{\partial S}\right|_T + \left.\frac{\partial J}{\partial \rho}\right|_q \left.\frac{\partial \rho}{\partial S}\right|_T = \beta\rho\left.\frac{\partial J}{\partial \rho}\right|_q. \quad (12)$$

Here β is the haline contraction coefficient. From (11), we can isolate the sensitivity of J to temperature due to the dynamic influence on density:

$$\left.\frac{\partial J}{\partial T}\right|_q = -\alpha\rho\left.\frac{\partial J}{\partial \rho}\right|_q = -\frac{\alpha}{\beta}\left.\frac{\partial J}{\partial S}\right|_T. \quad (13)$$

Combining (11) and (12), we obtain the sensitivity to temperature due to advection and diffusion:

$$\left.\frac{\partial J}{\partial T}\right|_\rho = \left.\frac{\partial J}{\partial T}\right|_S + \frac{\alpha}{\beta}\left.\frac{\partial J}{\partial S}\right|_T. \quad (14)$$

3. Model configuration and experiments

The Regional Ocean Modeling System is a terrain-following coordinate primitive equation model in widespread use for coastal and continental shelf applications (Haidvogel et al. 2008). The ROMS computational kernel (Shchepetkin and McWilliams 1998, 2003, 2005) uses high-order time stepping and advection and a carefully designed temporal averaging filter to guarantee exact conservation and constancy preservation for tracers and momentum and to minimize the aliasing of unresolved barotropic signals into the slow baroclinic motions. The model domain shown in Fig. 1 spans the area from south of Delaware Bay northward to eastern Long Island and from the coast out to about 60 m deep on the continental shelf. The Hudson and Delaware Rivers are included. The model has 30 vertical layers and horizontal resolution of about 1 km. Circulation in the apex of New York Bight is mainly locally driven (Zhang et al. 2009), so gradient open boundary conditions are applied on all open boundaries.
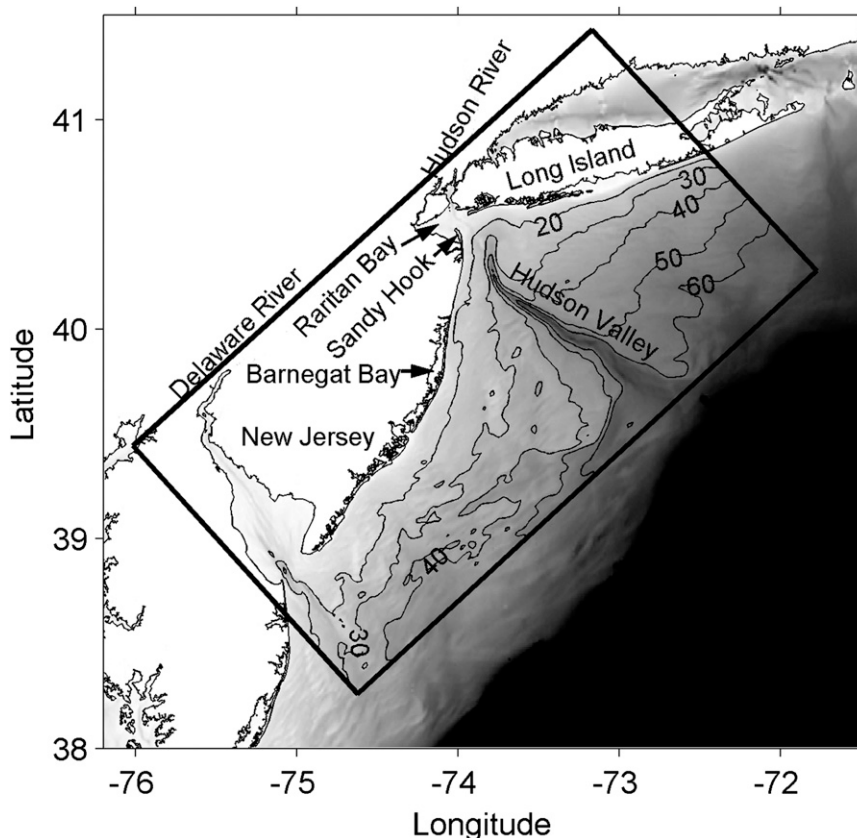
FIG. 1. Model domain (black frame) and bathymetry of the New York Bight. Depth contours
are in meters.

Forcing scenarios are idealized in this study to de-
velop experience with the adjoint model while also
studying the regional ocean dynamics: Here, tides and
surface water exchange are neglected and both rivers
have a steady discharge of 500 m^3 s^{-1}, which is typical
outside of high discharge storm or freshet events. Be-
cause we are focusing on the oceanic dynamical up-
stream in this study, the surface heat exchange, an ap-
parent factor for SST variation, is simply neglected. We
conduct three adjoint sensitivity experiments to study
the buoyancy-driven coastal circulation and wind-driven
upwelling and downwelling that are major features of
the dynamics in this area. In experiment 1, no surface
wind is applied, and a coastal current is generated by
river buoyancy input. In experiment 2, both river input
and a southward 5 m s^{-1} wind are applied. The wind is
switched to northward and coastal upwelling is gener-
ated in experiment 3. The initial conditions for the
spinup of these experiments are from the corresponding
model outputs of Choi and Wilkin (2007) in which the
ocean has had three months to adjust to a realistic state.
The SST and surface current at the end of 3-day spinup
periods for the respective experiments are shown in

Fig. 2; the patterns are similar to those identified by
Choi and Wilkin for these forcing scenarios.

The adjoint and tangent linear component models
for ROMS, together with drivers that link these models
for adjoint sensitivity, optimal perturbation, incre-
mental strong constraint four-dimensional variational
(IS4DVAR) and weak constraint 4DVAR (W4DVAR)
data assimilation have been developed by the ROMS
Adjoint Group (Di Lorenzo et al. 2007; Moore et al.
2004). The adjoint sensitivity driver runs the ROMS
adjoint model backward in time with zero initial con-
dition. Adjoint forcing is prepared offline and given to
the model.

The validity of the tangent linearization should be
verified prior to performing an adjoint sensitivity anal-
ysis. This is done by using the ROMS optimal pertur-
bation driver, based on general stability theory (Farrell
and Moore 1992; Moore and Farrell 1993), to first ob-
tain the perturbation to initial conditions that has the
most rapid energy growth among all singular vectors of
the tangent linear system. The perturbation pattern is
then scaled by a factor to give the initial condition per-
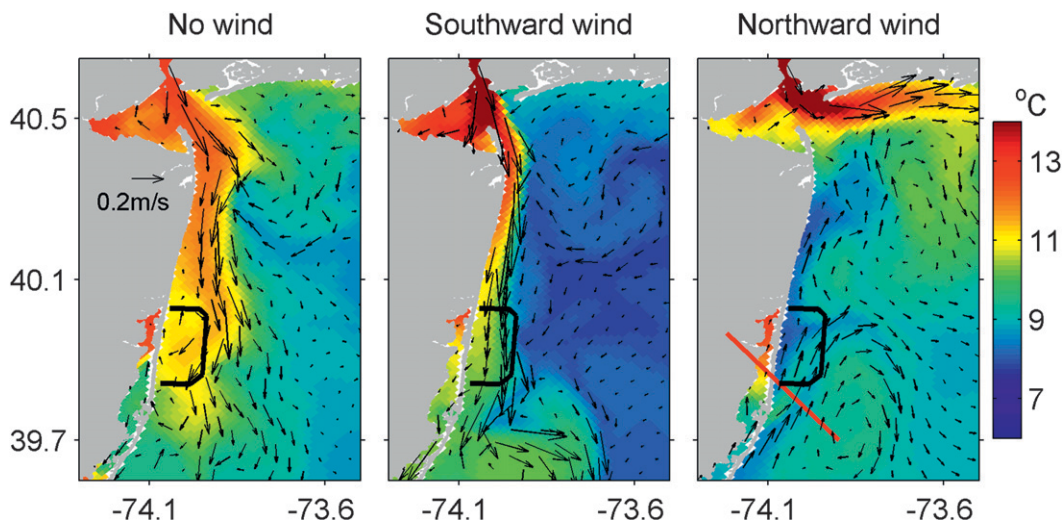turbation a magnitude characteristic of model uncertainty

FIG. 2. Forward model SST and surface current at the end of the 3-day period for expts 1 (no wind), 2 (southward wind), and 3 (northward wind). The thick black frame indicates the adjoint sensitivity region *A*. The red line in the right-hand figure indicates the location of the cross section in section 4c.

(0.3 m s^{-1} for velocity, 0.2°C for temperature, 0.2 for salinity) in this area. Three simulations are conducted for each experiment: the first is the control case and is the nonlinear forward simulation used as the base state of the adjoint model; the second, a perturbed nonlinear model, has the scaled perturbation added to the initial conditions of the control simulation; the third, a tangent linear model, is initialized with the scaled perturbation itself. The difference of the nonlinear forward models (perturbed minus control) is compared with the corresponding tangent linear model solution, and the similarity is evaluated by centered pattern correlation analysis (Santer et al. 1993). Figure 3 shows the comparison for experiments 2 and 3. For experiment 1 (not shown) the similarity is much higher, presumably because of the absence of wind-induced mixing. The similarity of nonlinear and tangent linear solutions for experiments 2 and 3 decreases gradually from 1 as time advances and the accumulated effects of nonlinearity become important. After 3 days, the correlation is about 0.6 for southward wind (experiment 2) and about 0.8 for northward wind (experiment 3). Therefore, we are confident the linearization around the nonlinear model trajectory is valid for the 3-day duration time window of the adjoint model simulations presented here.

4. Model output and discussion

a. Experiment 1: No wind

In the nonlinear forward model of this experiment, a purely buoyancy-driven coastal current is generated. As shown in Fig. 2a and examined in detail by Choi and

Wilkin (2007), when the Hudson River volume discharge is modest a low salinity plume exits Raritan Bay and flows southward along the New Jersey coast. The current separates from the coast at about 40.2°N but southward flow continues on the eastern side of a weak anticyclonically recirculating feature. SST is higher at the coast than offshore owing to warm river water within the plume.

In the absence of wind, vertical mixing is low, and we anticipate that the coastal SST will be largely determined by the advection of temperature from upstream. We test this hypothesis using the SST anomaly adjoint sensitivity function *J*, introduced in Eq. (9), evaluated
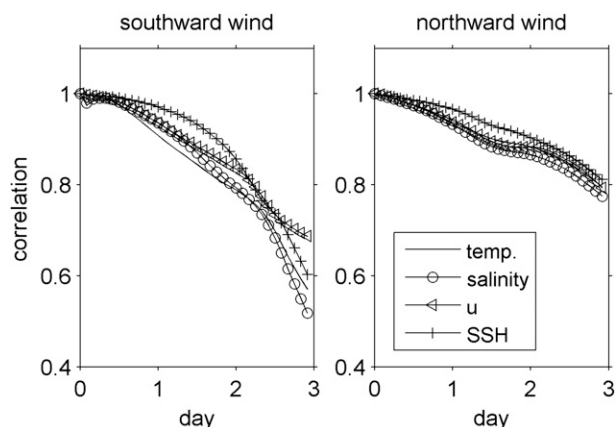

FIG. 3. Pattern correlation between the tangent linear model solution and the difference of two nonlinear model solutions (perturbed minus control; see text) for two idealized configurations: (left) southward and (right) northward wind. High correlation indicates validity of the tangent linear approximation.
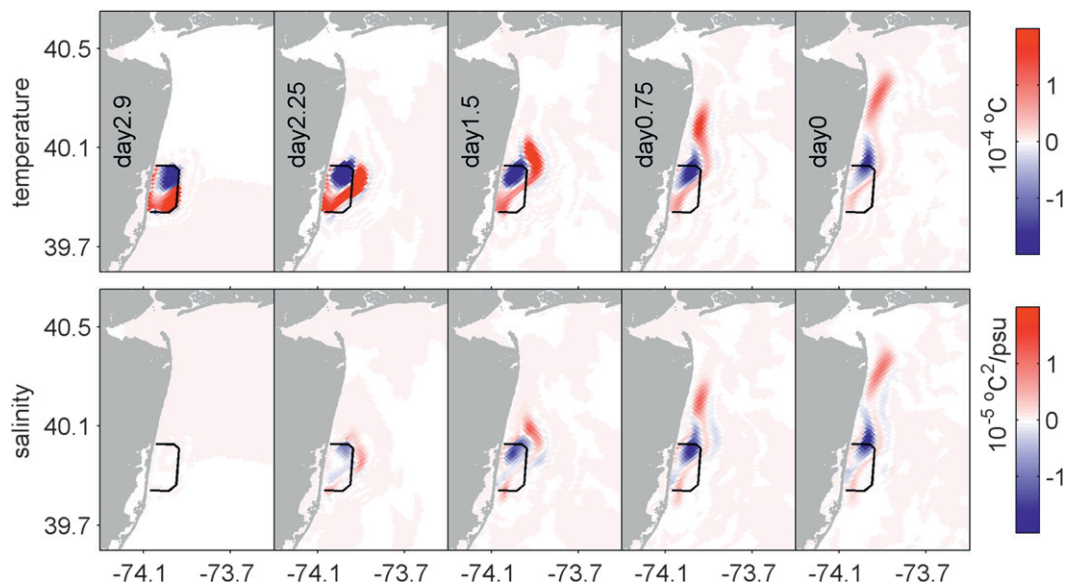
FIG. 4. Sensitivity of J to surface (top) temperature and (bottom) salinity at different times during the 3-day period for expt 1 (no wind). Time retreats backward from left to right. The region A over which J is evaluated, that is, the adjoint forcing area, is indicated by the black frame.

for the area A adjacent to the coast, indicated by the thick black frame in each panel of Fig. 4, and for a time interval t_1 to t_2 that spans the final 3 h of the 3-day window. The adjoint variables ($\partial J/\partial T$ and $\partial J/\partial S$) show how SST in region A at the end of the time window is influenced by the distribution of temperature and salinity in the preceding 3 days.

Figure 4 shows the evolution, backward in time (from left to right), of this temperature and salinity sensitivity evaluated at the surface. Surface values are plotted because the circulation is predominantly horizontal in this instance, although we emphasize that the adjoint variables are defined over all three spatial dimensions. As we shall see below, this can be particularly instructive for deducing three-dimensional transport pathways. The sensitivity to surface temperature (Fig. 4, top row) at day 2.9 is simply the temperature anomaly pattern within region A that determines J; it is proportional to $T_S - \overline{T}_S$. This is apparent if one considers the derivative of (9) with respect to T_S. The pattern shows positive sensitivity (anomaly) in the southern half of A and negative in the north.

As time proceeds backward, the southern part makes a cyclonic motion first, stretches out, and moves northward following the track of the river plume (Fig. 2a). The zone of maximum positive sensitivity lies at Sandy Hook on day 0 with a trail of sensitivity along almost the entire plume track. This means that surface temperature throughout most of the river plume on day 0 contributes to the surface temperature anomaly in region A three

days later; but the leading contribution comes from waters immediately southeast of Sandy Hook, so this can be considered the principal upstream source location. Sensitivity greater than zero means that higher plume temperatures on day 0 at Sandy Hook would give a stronger SST anomaly in the frame (i.e., larger J) on day 3. In contrast, the negative sensitivity patch in the northern half of the frame persists for the whole period. From Fig. 2a we can see that this region is relatively cool and static, being surrounded by warmer waters of the detached plume, which evidently trap the cool anomaly in place. The cool waters also contribute to J because it is defined as the square of SST anomaly, but the gradient of J with respect to SST there is negative. This states that, had cooler waters in the northern part of A been warmer during days 0 to 3, J would decrease. This is consistent with warming making the cool anomaly and plume temperatures more similar, decreasing the anomaly within A and thereby decreasing J.

A significant role of advection in driving the coastal SST anomaly is evident from the sensitivity to surface salinity shown in the bottom row of Fig. 4. Sensitivity to salinity starts from zero since changes in salinity will not affect J at the time for which it is defined. Proceeding backward in time, salinity sensitivity gradually grows along the plume track, eventually exhibiting a pattern very similar to the sensitivity to SST. Using Eqs. (12)–(14), the sensitivity to density, sensitivity to temperature associated with density effects, and sensitivity to temperature via passive advection are shown in
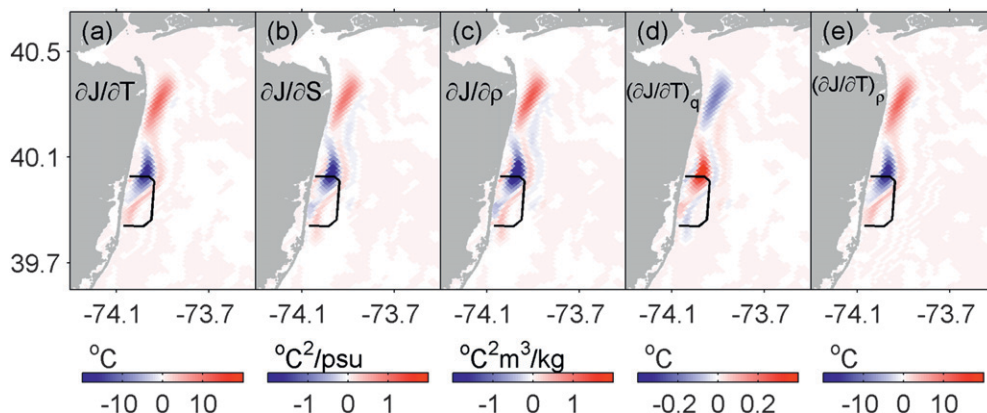
FIG. 5. Sensitivity, evaluated at the sea surface, of J with respect to (a) temperature, (b) salinity, (c) density, (d) temperature density effect, and (e) temperature advection and diffusion effect on day 0 of expt 1 (no wind): (a) and (b) are the full adjoint variable, (c) is computed using with Eq. (12), and (d) and (e) are computed with Eqs. (13) and (14), respectively. All the fields here are multiplied by 10^5.

Figs. 5c–e. Temperature sensitivity due to density-related effects is about two orders of magnitude smaller than the sensitivity due to advection. We conclude that the sensitivity of SST anomaly is dominated by advection, and the pattern shows clearly the trajectory of the source waters over the preceding three days.

The similarity in the patterns of sensitivity to surface salinity and temperature on day 0 (Fig. 4) is striking. To reveal the physical mechanism that leads to this, we make a small 0.01 salinity perturbation to the nonlinear

forward model surface initial condition and trace its impact on the circulation. The perturbation is placed southeast of Sandy Hook where sensitivity to salinity is greater than 5×10^{-6} °C^2. Figure 6 shows the evolution through time of the difference between the perturbed and unperturbed solutions for surface current and salinity (top row) and surface temperature (bottom row). As we would expect from the adjoint sensitivity results (Fig. 4), a positive salinity perturbation to the initial condition produces an increase in SST in the southern
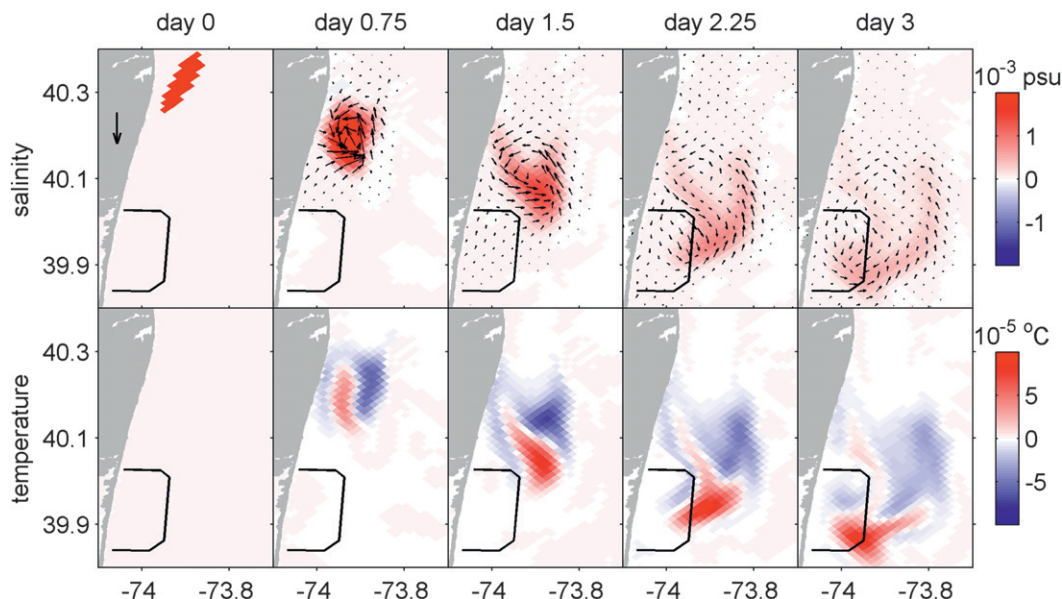

FIG. 6. The difference in nonlinear forward model simulations when a 0.01 salinity perturbation is added to the surface initial conditions in the region shown in the top left panel: (top) surface current difference superimposed on surface salinity difference and (bottom) surface temperature difference. The arrow in the top left panel is a scale for 10^{-5} m s^{-1}.
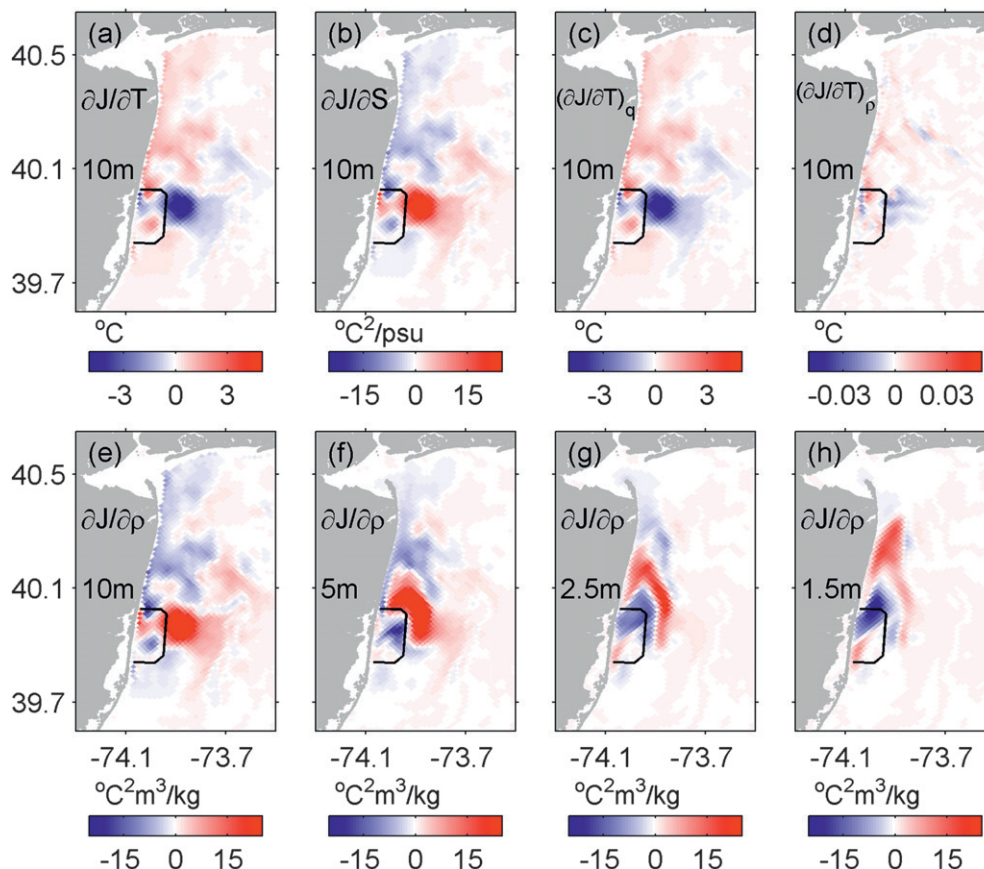
FIG. 7. Expt 1 (no wind): (top) sensitivity to (a) temperature, (b) salinity, (c) temperature density effect, and (d) temperature advection effect at 10-m depth and (bottom) sensitivity to density at different depths: (e) 10, (f) 5, (g) 2.5, and (h) 1.5 m. All plots are for the sensitivity of J at the beginning (day 0) of the 3-day period. The adjoint forcing area is indicated by the black frame. All fields here are multiplied by 10^6.

half of the sensitivity area A that increases J. Throughout the three days, the positive salinity anomaly always coincides with surface convergence anomaly and a dipole of positive and negative SST anomaly. At day 1 there is also more vertical sinking at the location of the salinity anomaly (not shown). Because Eq. (12) shows that sensitivity to salinity is positively related to sensitivity to density, we propose that the mechanism behind the positive sensitivity of SST to surface salinity is that the associated density anomaly introduces a convergent baroclinic pressure gradient anomaly that drives flow convergence and sinking and evolves a cyclonic circulation anomaly. This process suppresses vertical upward mixing and pulls warm plume water in from the west and cold mixed water in from the east toward the perturbation site, producing the dipole pattern of SST anomaly. This warmed surface water moves into the southern half of A and augments J.

However, the control mechanism is different beneath the surface. Figures 7a and 7b show sensitivity on day 0

to salinity and temperature at 10-m depth. Temperature sensitivity has opposite sign everywhere to the sensitivity to salinity and its absolute value is about five times smaller. Equation (12) is used to separate the density and advection effects at 10 m (Figs. 7c and 7d, respectively). Clearly, the sensitivity due to temperature density effect dominates at this depth—the role of advection or diffusion is minor. To explore this further, we show sensitivity to density on day 0 at depths of 10 m, 5 m, 2.5 m, and 1.5 m in Figs. 7e–h. At depth, there is a strong positive sensitivity to density close to the sensitivity region. Moving up through the water column, this region is displaced progressively farther upstream along the plume trajectory, consistent with a vertically sheared flow. We interpret this as showing, for each depth, the horizontal location where water at that depth affects vertical mixing of water into the sensitivity region. The sensitivity is positive because more dense subsurface water corresponds to stronger stratification; this suppresses the mixing of cold water up to the surface,
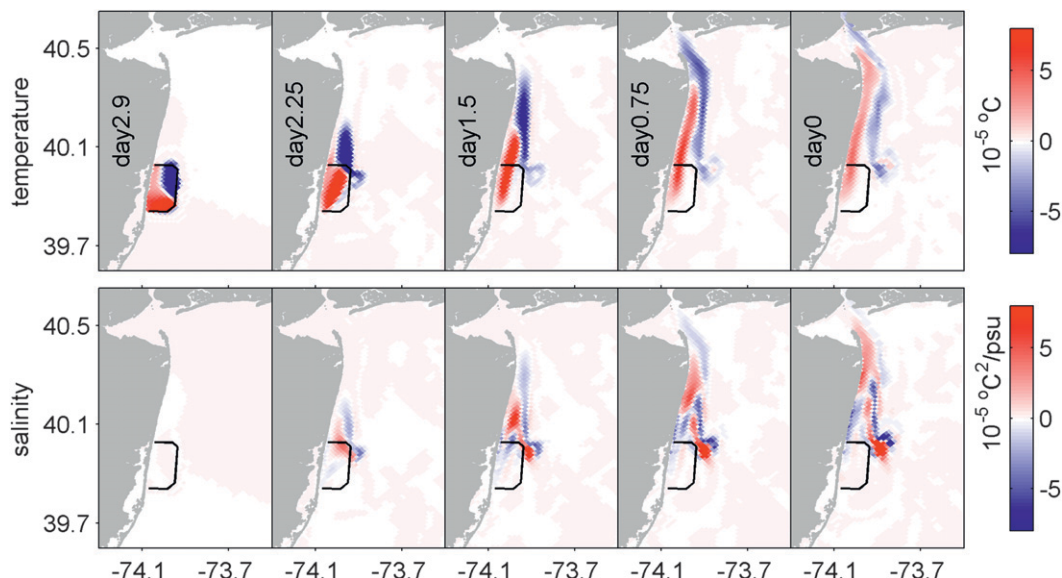
FIG. 8. Expt 2 (southward wind): sensitivity of *J* to surface (top) temperature and (bottom) salinity at different times during the 3-day period. Time retreats backward from left to right. The region *A* over which *J* is evaluated is indicated by the black frame.

causing a warmer plume and eventually higher SST anomaly in the sensitivity region on day 3. The opposite effect occurs in the colder part of the frame where warmer surface water would decrease *J* as in Fig. 5: denser water at that depth suppresses upward mixing, keeps the surface water warmer (surface cool water is still warmer than subsurface water), and decreases *J*, as shown by negative sensitivity to density in Figs. 7g,h.

b. Experiment 2: Southward downwelling wind

In experiment 2, a moderate 5 m s^{-1} southward wind blows over the entire domain for 20 days. Onshore Ekman transport pushes the river plume against the New Jersey coast, drives downwelling at the coast, and generates a geostrophically balanced southward coastal jet (Choi and Wilkin 2007) that augments the river plume as shown in Fig. 2b. Stronger vertical mixing is expected due to the effect of the wind, and there should be more water from offshore joining the plume along its path and eventually entering our chosen sensitivity area *A*. A time sequence of sensitivity of *J* to SST (Fig. 8) shows backward, or upstream, propagation that is faster and along a path closer to the coast than for the unforced plume of experiment 1.

In common with experiment 1, on day 3 the pattern of sensitivity to SST has positive value in the southern half of region *A* and negative in the north. Both features propagate, backward in time, along the plume track. The negative branch enters Raritan Bay and the Hudson River mouth with a long trail on the east side

of the plume, whereas the positive part stays in the coastal plume. A small persistent patch of sensitivity to SST lies just outside the northeastern corner of region *A* on day 0. This feature is more obvious in the sensitivity to surface salinity. Once again we separate the density and advection effects on day 0 using Eqs. (13) and (14) (Fig. 9). This shows that the positive and negative sensitivity to SST within and adjacent to the plume trajectory are both due mainly to temperature advection, whereas the patch at the northeastern corner of the frame is associated mostly with the influence of temperature on density and vertical mixing.

Revisiting Fig. 8, we now see that surface water in region *A* consists of three water sources: (i) river plume water that is already at the coast on day 0, (ii) a mixture of new water originating from the Hudson River after day 0 with cool surface water from east of the plume, and (iii) offshore surface water at the northeast corner of the frame on day 0. The first two water sources affect the SST anomaly in the frame mainly through advection. Because the first source is warmer than mean SST in the frame on day 3, sensitivity of *J* to this part of the upstream temperature is positive. The second source is opposite in sign because it is colder than mean SST in the frame. For surface water at the northeast corner of the frame on day 0, because the density effect there is dominant and it is colder than the average, *J* would be larger if stratification there decreased and vertical mixing was enhanced. Therefore, the sensitivity of *J* to the temperature of this patch of surface water is negative (Fig. 9).
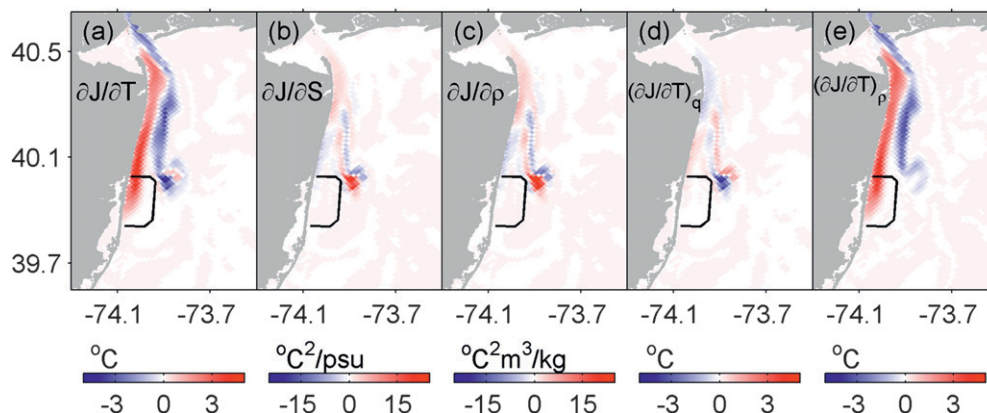
FIG. 9. Sensitivity, evaluated at the sea surface, of J with respect to (a) SST, (b) surface salinity, (c) density, (d) temperature density effect, and (e) temperature advection and diffusion effect on day 0 of expt 2 (southward wind). All fields here are multiplied by 10^5.

c. Experiment 3: Northward upwelling wind

In experiment 3, a uniform 5 m s^{-1} wind blows to the north and pushes the river plume toward Long Island (Fig. 2c). Along the New Jersey coast, offshore Ekman transport upwells deeper water to the surface (Choi and Wilkin 2007) and generates a coastal cold anomaly. Upward tilt of the thermocline and halocline at the coast associated with coastal upwelling can be seen in the temperature and salinity cross section (Fig. 11, top) along the red line in Fig. 2c. Note that a relative low temperature and salinity difference in the vertical is expected because the strong surface heating, charac-

teristic of summertime conditions in the NYB, is omitted, and there has been upwelling for a relatively long period during the spinup, which lowers vertical differences. In terms of the contribution to SST anomaly, strong vertical mixing due to deep cold water brought up to the surface lowers the contribution from upstream water temperature advection. Figure 10 shows sensitivity of J to SST and surface salinity in the same format as Figs. 4 and 8 for the previous experiments. The sensitivity to SST at day 2.9, which we note again is simply the initial temperature anomaly $T_S - \overline{T}_S$, has three patches: negative sensitivity at the northern and southern ends of the frame and positive in the middle. Both
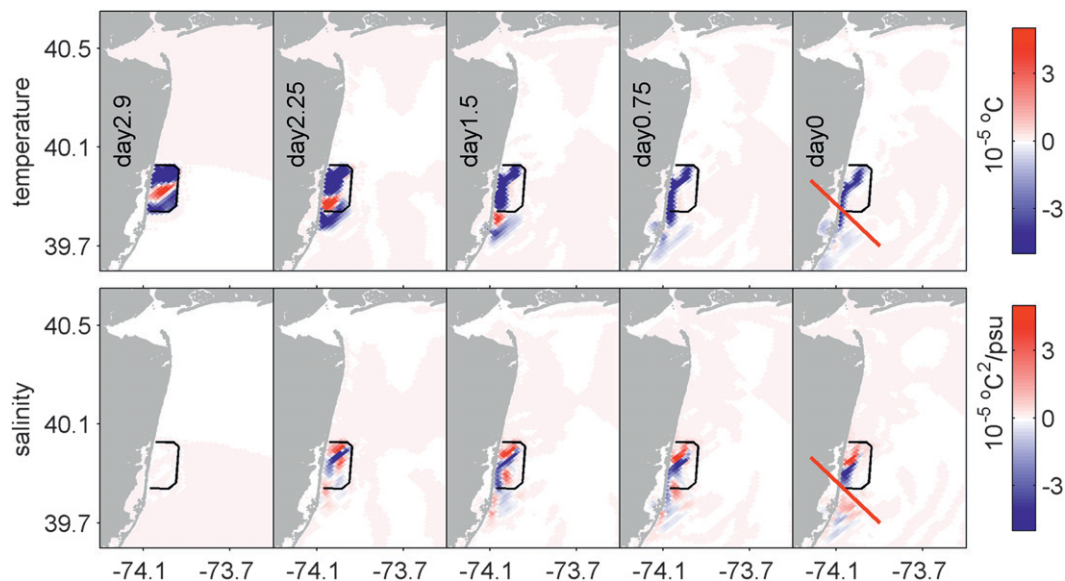

FIG. 10. Sensitivity of J to surface (top) temperature and (bottom) salinity through time for expt 3 (northward wind). The red line in the rightmost panel indicates the position of the vertical cross section for Fig. 11.

the negative and positive sensitivity signals in the south move southward as time proceeds backward (in the upstream direction for the upwelling coastal jet) but disappear rather rapidly compared to experiments 1 and 2; and the negative sensitivity in the north remains on the surface, and within the frame, through day 0. Thus, the surface water in the frame on day 3 actually has water sources on day 0: water deep in the southern end of the frame and previously upwelled, offshore moving water (see the cool tongue in Fig. 2). Almost the entire southeast half of region A shows zero sensitivity to temperature on day 0 because these waters are swept out of the frame by Ekman transport and make no contribution to SST on day 3.

To illustrate how adjoint sensitivity reveals the deep source of upwelling waters, cross sections of sensitivity to temperature and salinity, along the red line in Fig. 10, are shown in Fig. 11, along with cross sections of the forward model temperature and salinity. Because of the stretched ROMS vertical coordinate the sensitivity here is scaled by the local vertical grid spacing to remove effects of the discrete grid size (section 2b). Sensitivity to temperature and salinity gradually propagate to the deep and reach almost to the seafloor on day 0. At that time, both temperature and salinity sensitivity show a two-layer pattern parallel to the thermocline. Applying Eqs. (13) and (14), the roles of density and advection in the temperature sensitivity are separated in Fig. 12. These effects exert their influence at different depths: the sensitivity due to the dynamic role of density is positive and occurs mostly below 5 m, whereas above this there is negative sensitivity due to upwelling advection. A simple volume conservation calculation for the Ekman layer divergence indicates 5 m as the approximate distance the water would move vertically in 3 days. The sensitivity of J to temperature in the surface 5 m is negative because upwelling brings cold water to the surface and strengthens the southern cold anomaly in the frame. The reason for little dynamic density effect in this layer is presumably that small density changes to the water in the upper 5 m at day 0 cannot prevent the water from upwelling; the flow divergence is set by the wind stress. However, for the water beneath 5 m, SST at day 3 can be influenced through the effect of density stratification on vertical mixing and subsequently on the SST anomaly.

Sensitivity to density exhibits a two-layer pattern with negative sensitivity lying beneath positive sensitivity (Fig. 12c). To confirm this pattern, we follow an approach similar to that presented in Fig. 6 and add a 0.01 salinity perturbation at these layers in the initial conditions of a forward model run. The differences in SST between perturbed and unperturbed nonlinear model
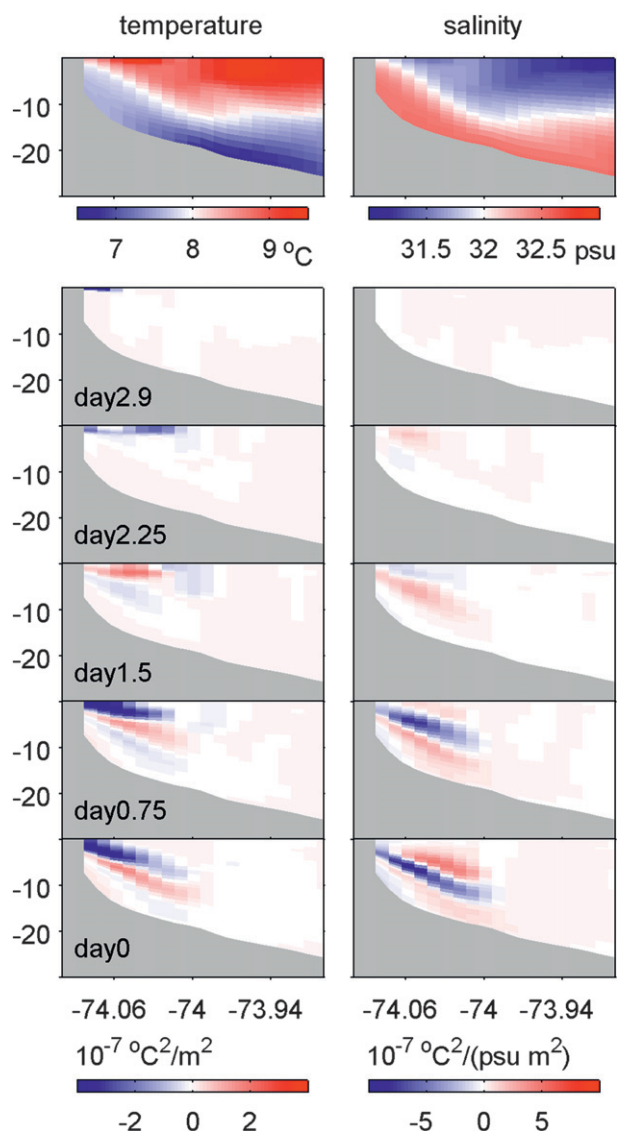

FIG. 11. (top) Forward model temperature and salinity along the vertical cross section indicated in Fig. 2c and Fig. 10; (bottom) sensitivity to (left) temperature and (right) salinity along the cross section at different times during the 3-day period for expt 3 (northward wind).

solutions on day 3 are shown in Fig. 13 for perturbations to the lower and upper layer, respectively. Both figures show a tripole pattern of SST anomalies with two positive patches bracketing a negative patch between them. Scrutiny of model state differences at other times (not shown) reveals that these patches originate subsurface and outcrop owing to uplift driven by the diverging Ekman transport. The pattern is displaced farther offshore for the salinity initial perturbation placed in the upper layer (Fig. 13b), and the impact on SST anomaly differs: the outcome of the lower layer perturbation (Fig. 13a) lowers the SST anomaly in the frame at
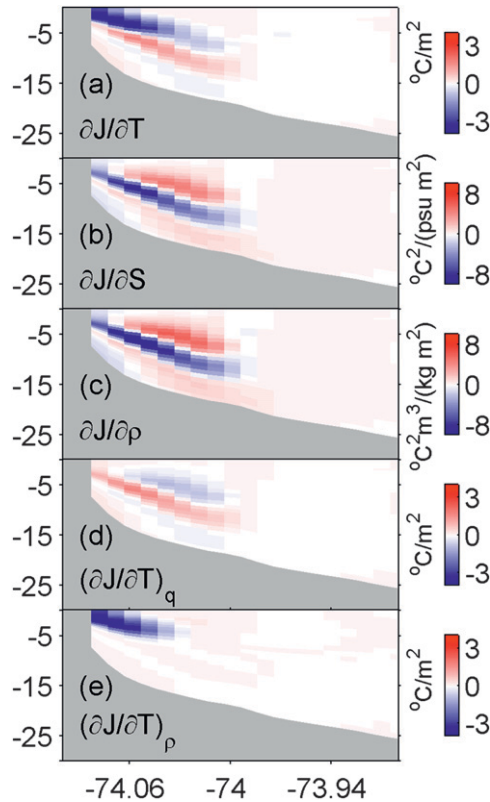
FIG. 12. Sensitivity to (a) temperature, (b) salinity, (c) density, (d) temperature density effect, and (e) temperature advection and diffusion effect along the vertical cross section indicated in Fig. 10 on day 0 of expt 3 (northward wind). All fields are multiplied by 10^7.

day 2.9 (see Fig. 10), and then sensitivity of J to salinity at that layer is negative; the upper layer perturbation (Fig. 13b) enhances the SST anomaly in the frame and then sensitivity of J to salinity in that layer is positive.
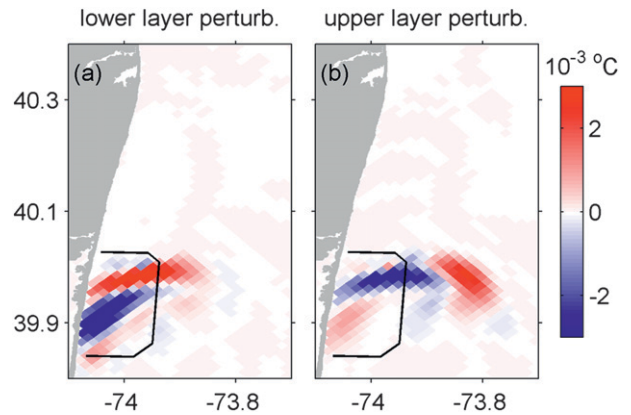

FIG. 13. Difference in SST in forward model simulations when a salinity perturbation is added as initial conditions to the (a) upper and (b) lower layer, for expt 3 (northward wind).

d. Comparison of the different contributions to total δJ

In addition to sensitivity to temperature and salinity, the adjoint model also gives the sensitivity of J to other state variables, forcing, and parameters of the model. To quantitatively compare the different contributions to the total variation of J, terms in Eq. (8) are estimated for all three experiments and shown in Table 1. For experiment 1 (no wind), the contribution of surface temperature dominates. Mixing is weak in this free river plume scenario, and the SST anomaly in the frame is determined principally by advection of warm water from upstream. From the perspective of observing system design, a good estimation of upstream water temperature along the New Jersey coast over the preceeding three days is highly relevant to knowledge of the SST anomaly in region A.

TABLE 1. Comparison of the magnitude of different contributions to J (coastal SST anomaly) for each of the three experiments: X denotes model variable or parameter (SI units), $\partial J/\partial X$ is the adjoint sensitivity (units $°C^2/[X]$), and δX is a typical small variation of X (units $[X]$).

Expt	X	Upstream temperature	Density	Surface current	Sea surface height	Vertical mixing of momentum	Vertical mixing of tracers	Wind stress
No wind	$\partial J/\partial X$	1×10^{-4}	10^{-5}	2×10^{-4}	3×10^{-5}	1	0.3	10^{-4}
	δX	2	1	10^{-1}	10^{-2}	10^{-5}	10^{-6}	–
	$\frac{\partial J}{\partial X}\delta X\ (°C^2)$	2×10^{-4}	10^{-5}	2×10^{-5}	3×10^{-7}	10^{-5}	3×10^{-7}	–
Southward wind	$\partial J/\partial X$	5×10^{-5}	2×10^{-4}	5×10^{-4}	3×10^{-4}	10	3×10^{-2}	5×10^{-4}
	δX	2	1	10^{-1}	10^{-2}	10^{-5}	10^{-4}	5×10^{-3}
	$\frac{\partial J}{\partial X}\delta X\ (°C^2)$	10^{-4}	2×10^{-4}	5×10^{-5}	3×10^{-6}	10^{-4}	3×10^{-6}	2.5×10^{-6}
Northward wind	$\partial J/\partial X$	1×10^{-4}	2×10^{-4}	5×10^{-4}	2×10^{-4}	5×10^{-1}	10^{-2}	3×10^{-4}
	δX	2	1	10^{-1}	10^{-2}	10^{-5}	10^{-4}	10^{-3}
	$\frac{\partial J}{\partial X}\delta X\ (°C^2)$	2×10^{-4}	2×10^{-4}	5×10^{-5}	2×10^{-6}	5×10^{-6}	10^{-6}	3×10^{-7}

For experiment 2 (southward wind), Table 1 shows that density makes the leading contribution, followed by upstream temperature advection and vertical mixing. The contribution of wind to SST anomaly variation over the three days is surprisingly small considering that the strong coastal current is mainly due to the downwelling favorable wind. An adjoint model simulation that we have run with a longer time window does show sensitivity to wind stress having a leading role in the variation of J. We interpret this as indicating that the full strength of the coastal current takes several days to evolve and is not strongly impacted by wind changes in the last three days of simulation. Once established, details of the SST patterns within the current itself become the main contributor to variation of the J defined here.

The same logic applies to experiment 3, the upwelling scenario, for which Table 1 shows density and upstream temperature advection as the largest contributors. A leading contribution from density is to be expected because changes to the vertical stratification can alter both mixing and the depth from which upwelled water is drawn (Allen et al. 1995). Both of these influences can change SST, as explained in section 4c, on the 3-day time scale. Therefore, in this circulation scenario, observation of the vertical density distribution as well as the upstream water temperature over the preceding three days is significant for accurate simulation of the SST anomaly at the end of the period.

The quantitative comparison of the relative contributions of different state variables and forcing variables under different circulation scenarios, together with the spatially and temporally resolved adjoint sensitivity information in sections 4a–c, sheds light on the timing and location of variations in the ocean state that are crucial for precise prediction of the future SST anomaly conditions as characterized by J. Observation of these variables at the identified times and locations can reasonably be expected to be of significantly greater value when seeking to adjust the model prior state through data assimilation.

5. Summary

As a step toward building a coastal ocean forecast system for the New York Bight, we have undertaken an adjoint model study of the sensitivity of New Jersey coastal SST anomalies for three idealized wind forcing scenarios: no wind, upwelling-favorable, and downwelling-favorable wind. The adjoint sensitivity formulas were derived first to clarify how adjoint sensitivity has the capability to simultaneously compare the contribution from different state variables, model forcing, and model parameters to the variation of some chosen model aspect

characterized via a scalar functional J and then identify the main source of that variation.

To focus on characteristics of short-term wind-induced SST anomalies adjacent to the New Jersey coast, our scalar functional J was defined as the temporal and spatial mean of the square of SST anomaly in a frame area of a small central sector of the New Jersey coast for a brief prescribed time interval. Within this definition, ocean temperature can affect J through two different processes: the advection and diffusion of source waters of differing temperature into the frame region and the effect that temperature has on circulation and mixing through its contribution to density. It was shown that these influences can be separated by deriving a decomposition based on applying the chain rule to the adjoint sensitivity analysis; the method essentially exploits the density information in the sensitivity to salinity at constant temperature. Prior to the adjoint sensitivity analysis, we verify that the linearization assumption of the adjoint model is valid by comparing the tangent linear model solution with the difference between two, slightly perturbed, nonlinear model solutions. The tangent linearization is valid for the 3-day time window of this study. Care is taken to normalize the adjoint sensitivity appropriately to remove effects of the vertical grid discretization before interpretation of the results.

In the first experiment, the Hudson River discharge generates a purely buoyancy-driven coastal current in the nonlinear model (no wind). The adjoint sensitivity method shows that of all ocean state variables (temperature, salinity, velocity) and forcing, throughout the entire model domain and at all preceding times, temperature itself has the greatest impact on J in this experiment. The decomposition of sensitivity into advection and density contributions shows that in this scenario advection dominates over the indirect role of temperature on circulation exerted through the influence of density on mixing and pressure gradients. The sensitivity of J to surface temperature identifies two sources of the surface water in the frame where the functional J is defined: warm plume water and cooler coastal ocean water that is partially surrounded by the river plume where it detaches from the coast. Analysis of the sensitivity to subsurface water temperatures shows these exert their influence principally through the dynamic density effect.

In experiment 2, a 5 m s^{-1} southward wind blows and drives a strong coastal current in the same direction as the buoyancy-driven circulation. Adjoint sensitivity highlights three significant sources of influence on J. Decomposition shows that two stretches of water parallel to the coast and of opposite sign in sensitivity act through temperature advection, while a small patch northeast of

the sensitivity frame influences SST less directly owing to the dynamic effect of density.

Deep water is uplifted to the surface in experiment 3 due to a northward upwelling-favorable wind. The sensitivity of J to SST rapidly diminishes at the coast as time proceeds backward in this scenario because surface waters to the south are swept offshore by Ekman transport and do not enter the sensitivity region where J is defined. A vertical cross section of sensitivity to temperature confirms that there is a deep source of the temperatures that influence SST anomaly and clearly delineates its depth and offshore extent through time. Separation of the sensitivity to temperature into the respective contributions of advection and dynamics shows that the influence of direct advection is restricted to mainly the top 5 m layer of the water column and some 10 km offshore (3 days previously), whereas the indirect dynamic or density effect is beneath this layer (5 to 15 m depth) and over the same across-shelf extent.

The contributions from different variables and parameters to the total variation of J are quantitatively compared. For the no-wind, unforced plume experiment, the upstream surface temperature dominates. For the downwelling-favorable wind experiment, the density effect is shown to be the leading contribution, followed by temperature advection and vertical mixing. Only when adjoint simulations are extended to a time window longer than three days do we find that wind stress can become the dominant source of sensitivity for the chosen J. For the upwelling scenario, density and upstream temperature advection contribute equally to J. The importance of density is expected in this case because upwelling is against the vertical stratification and changes in vertical density structure alter details of the upwelling process and subsequently SST characterized by J.

The results obtained in this study demonstrate the ability of adjoint sensitivity to identify the oceanic conditions and forcing that are "dynamically upstream" to a region or feature of interest, water sources, the main contributors to variation of a defined model feature, and often the mechanisms behind these. The timing and location of variations in the ocean state that are crucial for subsequent prediction of the model features, as characterized by a chosen functional J, are clearly highlighted. It follows, therefore, that observation of these variables at the identified locations and times can be expected to have significant value when used to adjust the model prior state through data assimilation. This property embodied in the adjoint model will underpin future data assimilation and adaptive sampling studies.

REFERENCES

Allen, J. S., P. A. Newberger, and J. Federiuk, 1995: Upwelling circulation on the Oregon continental shelf. Part I: Response to idealized forcing. *J. Phys. Oceanogr.,* **25,** 1843–1866.

Bennett, A. F., 2002: *Inverse Modeling of the Ocean and Atmosphere.* Cambridge University Press, 234 pp.

Bertsekas, D. P., 1982: *Constrained Optimization and Lagrange Multiplier Methods.* Academic Press, 395 pp.

Castelao, R. M., S. Glenn, O. Schofield, R. J. Chant, J. Wilkin, and J. Kohut, 2008: Seasonal evolution of hydrographic fields in the central Middle Atlantic Bight from glider observations. *Geophys. Res. Lett.,* **35,** L03617, doi:10.1029/2007GL032335.

Chant, R. J., 2001: Evolution of near-inertial waves during an upwelling event on the New Jersey inner shelf. *J. Phys. Oceanogr.,* **31,** 746–764.

——, S. Glenn, and J. Kohut, 2004: Flow reversals during upwelling conditions on the New Jersey inner shelf. *J. Geophys. Res.,* **109,** C12S03, doi:10.1029/2003JC001941.

Choi, B.-J., and J. L. Wilkin, 2007: The effect of wind on the dispersal of the Hudson River plume. *J. Phys. Oceanogr.,* **37,** 1878–1897.

Courtier, P., J.-N. Thépaut, and A. Hollingsworth, 1994: A strategy for operational implementation of 4DVAR using an incremental approach. *Quart. J. Roy. Meteor. Soc.,* **120,** 1367–1387.

Di Lorenzo, E., A. M. Moore, H. G. Arango, B. D. Cornuelle, A. J. Miller, B. Powell, B. S. Chua, and A. Bennett, 2007: Weak and strong constraint data assimilation in the inverse Regional Ocean Modeling System (ROMS): Development and application for a baroclinic coastal upwelling system. *Ocean Modell.,* **16,** 160–187.

Dutkiewicz, S., M. Follows, P. Heimbach, and J. Marshall, 2006: Controls on ocean productivity and air–sea carbon flux: an adjoint model sensitivity study. *Geophys. Res. Lett.,* **33,** L02603, doi:10.1029/2005GL024987.

Errico, R. M., 1997: What is an adjoint model? *Bull. Amer. Meteor. Soc.,* **78,** 2577–2591.

——, and T. Vukicevic, 1992: Sensitivity analysis using an adjoint of the PSU–NCAR mesoscale model. *Mon. Wea. Rev.,* **120,** 1644–1660.

Farrell, B. F., and A. M. Moore, 1992: An adjoint method for obtaining the most rapidly growing perturbation to oceanic flows. *J. Phys. Oceanogr.,* **22,** 338–349.

Galanti, E., and E. Tziperman, 2003: A midlatitude–ENSO teleconnection mechanism via baroclinically unstable long Rossby waves. *J. Phys. Oceanogr.,* **33,** 1877–1888.

Garvine, R. W., 2004: The vertical structure and subtidal dynamics of the inner shelf off New Jersey. *J. Mar. Res.,* **62,** 337–371, doi:10.1357/0022240041446182.

Haidvogel, D. B., and Coauthors, 2008: Ocean forecasting in terrain-following coordinates: Formulation and skill assessment of the regional ocean modeling system. *J. Comput. Phys.,* **227,** 3595–3624.

Hill, C., V. Bugnion, M. Follows, and J. Marshall, 2004: Evaluating carbon sequestration efficiency in an ocean circulation model

by adjoint sensitivity analysis. *J. Geophys. Res.,* **109,** C11005, doi:10.1029/2002JC001598.

Johnson, D. R., J. Miller, and O. Schofield, 2003: Dynamics and optics of the Hudson River outflow plume. *J. Geophys. Res.,* **108,** 3323, doi:10.1029/2002JC001485.

Junge, M. M., and T. W. N. Haine, 2001: Mechanisms of North Atlantic wintertime sea surface temperature anomalies. *J. Climate,* **14,** 4560–4572.

Köhl, A., and D. Stammer, 2004: Optimal observations for variational data assimilation. *J. Phys. Oceanogr.,* **34,** 529–542.

Kohut, J., S. Glenn, and R. J. Chant, 2004: Seasonal current variability on the New Jersey inner shelf. *J. Geophys. Res.,* **109,** C07S07, doi:10.1029/2003JC001963.

Lewis, J. M., K. D. Raeder, and R. M. Errico, 2001: Vapor flux associated with return flow over the Gulf of Mexico: A sensitivity study using adjoint modeling. *Tellus,* **53A,** 74–93, doi:10.1034/j.1600-0870.2001.01108.x.

Li, X., and C. Wunsch, 2004: An adjoint sensitivity study of chlorofluorocarbons in the North Atlantic. *J. Geophys. Res.,* **109,** C01007, doi:10.1029/2003JC002014.

Losch, M., and P. Heimbach, 2007: Adjoint sensitivity of an ocean general circulation model to bottom topography. *J. Phys. Oceanogr.,* **37,** 377–393.

Marotzke, J., R. Giering, K. Q. Zhang, D. Stammer, C. N. Hill, and T. Lee, 1999: Construction of the adjoint MIT ocean general circulation model and application to Atlantic heat transport sensitivity. *J. Geophys. Res.,* **104,** 29 529–29 547.

Moore, A. M., and B. F. Farrell, 1993: Rapid perturbation growth on spatially and temporally varying oceanic flows determined using an adjoint method: Application to the Gulf Stream. *J. Phys. Oceanogr.,* **23,** 1682–1702.

——, H. G. Arango, E. Di Lorenzo, B. D. Cornuelle, A. J. Miller, and D. J. Neilson, 2004: A comprehensive ocean prediction and analysis system based on the tangent linear and adjoint of a regional ocean model. *Ocean Modell.,* **7,** 227–258.

——, ——, ——, A. J. Miller, and B. D. Cornuelle, 2009: An adjoint sensitivity analysis of the Southern California Current circulation and ecosystem. Part I: The physical circulation. *J. Phys. Oceanogr.,* **39,** 702–720.

Münchow, A., and R. J. Chant, 2000: Kinematics of inner shelf motions during the summer stratified season off New Jersey. *J. Phys. Oceanogr.,* **30,** 247–268.

Santer, B. D., T. M. L. Wigley, and P. D. Jones, 1993: Correlation methods in fingerprint detection studies. *Climate Dyn.,* **8,** 265–276.

Shchepetkin, A. F., and J. C. McWilliams, 1998: Quasi-monotone advection schemes based on explicit locally adaptive dissipation. *Mon. Wea. Rev.,* **126,** 1541–1580.

——, and ——, 2003: A method for computing horizontal pressure-gradient force in an oceanic model with a non-aligned vertical coordinate. *J. Geophys. Res.,* **108,** 3090, doi:10.1029/2001JC001047.

——, and ——, 2005: The Regional Oceanic Modeling System (ROMS): A split-explicit, free-surface, topography-following coordinate oceanic model. *Ocean Modell.,* **9,** 347–404.

Tilburg, C. E., and R. W. Garvine, 2003: Three-dimensional flow in a coastal upwelling zone: Alongshore convergence and divergence on the New Jersey Shelf. *J. Phys. Oceanogr.,* **33,** 2113–2115.

van Oldenborgh, G. J., G. Burgers, S. Venzke, C. Eckert, and R. Giering, 1999: Tracking down the ENSO delayed oscillator with an adjoint OGCM. *Mon. Wea. Rev.,* **127,** 1477–1496.

Wong, K.-C., 1999: The wind driven currents on the Middle Atlantic Bight inner shelf. *Cont. Shelf Res.,* **19,** 757–773, doi:10.1016/S0278-4343(98)00107-1.

Yankovsky, A. E., 2003: The cold-water pathway during an upwelling event on the New Jersey shelf. *J. Phys. Oceanogr.,* **33,** 1954–1966.

——, and R. W. Garvine, 1998: Subinertial dynamics on the inner New Jersey shelf during the upwelling season. *J. Phys. Oceanogr.,* **28,** 2444–2458.

——, ——, and A. Munchow, 2000: Mesoscale currents on the inner New Jersey shelf driven by the interaction of buoyancy and wind forcing. *J. Phys. Oceanogr.,* **30,** 2214–2230.

Zhang, W. G., J. L. Wilkin, and R. J. Chant, 2009: Modeling the pathways and mean dynamics of river plume dispersal in the New York Bight. *J. Phys. Oceanogr.,* **39,** 1167–1183.